Eigenstate thermalization and its breakdown in quantum spin chains with inhomogeneous interactions

Ding-Zu Wang ⬚,[1,*] Hao Zhu,[1,*] Jian Cui,[1] Javier Argüello-Luengo,[2] Maciej Lewenstein,[2,3]
Guo-Feng Zhang ⬚,[1,†] Piotr Sierant,[2,‡] and Shi-Ju Ran[4,§]

[1]*School of Physics, Beihang University, 100191 Beijing, China*

[2]*ICFO - Institut de Ciencies Fotoniques, The Barcelona Institute of Science and Technology, Av. Carl Friedrich Gauss 3,
08860 Castelldefels (Barcelona), Spain*

[3]*ICREA, Pg. Lluís Companys 23, 08010 Barcelona, Spain*

[4]*Center for Quantum Physics and Intelligent Sciences, Department of Physics, Capital Normal University, Beijing 10048, China*

The eigenstate thermalization hypothesis (ETH) is a successful theory that establishes the criteria for ergodicity and thermalization in isolated quantum many-body systems. In this work, we investigate the thermalization properties of a spin-1/2 *XXZ* chain with linearly inhomogeneous interactions. We demonstrate that introduction of the inhomogeneous interactions leads to an onset of quantum chaos and thermalization, which, however, becomes inhibited for sufficiently strong inhomogeneity. To exhibit ETH, and to display its breakdown upon varying the strength of interactions, we probe statistics of energy levels and properties of matrix elements of local observables in eigenstates of the inhomogeneous *XXZ* spin chain. Moreover, we investigate the dynamics of the entanglement entropy and the survival probability which further evidence the thermalization and its breakdown in the considered model. We outline a way to experimentally realize the *XXZ* chain with linearly inhomogeneous interactions in systems of ultracold atoms. Our results highlight a mechanism of emergence of ETH due to insertion of inhomogeneities in an otherwise integrable system and illustrate the arrest of quantum dynamics in the presence of strong interactions.

I. INTRODUCTION

Understanding the thermalization and equilibration in isolated quantum many-body systems has been a central topic since the birth of quantum mechanics [1,2]. Its growing interest is closely linked to the remarkable progress in the ultracold atomic experiments [3–5], where advancements in control and isolation have enabled the coherence in many-body systems over unprecedented time scales [6,7]. The experiments on nonequilibrium dynamics have revealed thermalization in the chaotic quantum systems [8–12], which is inhibited in the integrable systems [13–16].

Thermalization in generic (quantum-chaotic, nonintegrable) isolated quantum many-body systems can be explained by the eigenstate thermalization hypothesis (ETH) [17,18]. The ETH is usually formulated as an ansatz for matrix elements of physical observables in the eigenbasis of the Hamiltonian [17–20]. This ansatz guarantees that the local observables after relaxation can be described by appropriate ensembles of statistical mechanics, while the fluctuations in a steady state satisfy the fluctuation dissipation theorem [21]. Recently, the connections between the notions of *k* designs

[22], the theory of free probability [23], and ETH were made explicit [24–26].

The validity of the ETH ansatz has been confirmed in a wide range of quantum many-body systems, including spin chains, bosonic and fermionic models, or systems with electron-photon coupling [27–40]. One-dimensional spin-1/2 *XXZ* chain with various types of integrability breaking terms has become a paradigmatic system for studies of ETH [41–47]. Introduction of spatial inhomogeneities is an intriguing way of integrability breaking, especially considering its relevance to nonequilibrium physics [48–57] and generalized hydrodynamics [58–63].

In this work, we investigate the eigenstate thermalization properties of the spin-1/2 *XXZ* chain with spatially inhomogeneous interaction strength; see Fig. 1. The considered Hamiltonian consists of the spatially uniform hopping terms and inhomogeneous *z*-*z* spin coupling whose strength varies linearly across the chain. By means of exact diagonalization (ED), we show that the system is driven from an integrable point to a quantum chaotic region upon introduction of the linear variation of the *z*-*z* spin coupling. However, when the inhomogeneity becomes sufficiently strong, it inhibits the thermalization of the system.

This manuscript is structured as follows. In Sec. II, we detail the *XXZ* model with spatially inhomogeneous interactions. In Sec. III, we formulate our predictions about integrability and thermalization in the system by investigating its level statistics. Section IV contains a detailed study of ETH and its

---

*These two authors contributed equally to this work.

†Corresponding author: gf1978zhang@buaa.edu.cn

‡Corresponding author: Piotr.Sierant@icfo.eu
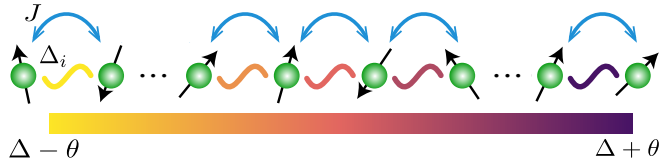
§Corresponding author: sjran@cnu.edu.cn

FIG. 1. Schematic representation of the *XXZ* chain with linearly varying z-z interactions. The uniform hopping term is denoted by J, while Δ_i represents an inhomogeneous z-z coupling whose strength varies linearly with the spatial position, as depicted by the color scheme in the figure. Interaction strength is $\Delta - \theta$ ($\Delta + \theta$) at the leftmost (rightmost) site of the chain.

breakdown in the considered model, with particular attention devoted to properties of the matrix elements of local operators. In Sec. V, we demonstrate qualitative changes in the dynamics of the system in the identified ETH and nonergodic regimes. Finally, Sec. VI details a blueprint proposal for realization of the considered model in cold atomic systems. We summarize our findings and provide an outlook in Sec. VII.

II. *XXZ* CHAIN WITH SPATIALLY INHOMOGENEOUS INTERACTION

We consider the spin-1/2 *XXZ* chain with inhomogeneous interaction and open boundary conditions (Fig. 1), whose Hamiltonian can be written as (putting $\hbar = 1$)

$$\hat{H}_{\text{inho}} = \sum_{i=1}^{N-1} \left[J(\sigma_i^x \sigma_{i+1}^x + \sigma_i^y \sigma_{i+1}^y) + \Delta_i \sigma_i^z \sigma_{i+1}^z \right], \qquad (1)$$

where σ_i^α represents the Pauli operator of the *i*th spin in the $\alpha \in \{x, y, z\}$ direction and N is the length of chain that is taken to be even. The *XXZ* spin chain can be mapped via the Jordan-Wigner transformation to a system of interacting spinless fermions, with the hopping strength equal to J and nearest-neighbor density-density interaction strength Δ_i. We set the hopping strength $J = 1$ as the energy unit. The strength of the z-z coupling terms is assumed to vary linearly with the spatial position as

$$\Delta_i = \Delta + \theta \frac{2i - N}{N - 2}, \qquad (2)$$

where θ is the slope of the linear dependence characterizing the strength of inhomogeneity and Δ represents the average interaction strength. A homogeneous *XXZ* chain will be obtained by taking $\theta = 0$, which is a quintessential interacting integrable model [64,65].

The Hamiltonian $\hat{H}_{\text{inho}}$ in Eq. (1) has the $U(1)$ symmetry as it conserves the total magnetization along the spin z direction, $[\hat{H}_{\text{inho}}, \sum_i \sigma_i^z] = 0$. The zero magnetization sector ($\sum_i \langle \sigma_i^z \rangle = 0$) is the largest sector that maintains the Z_2 spin inversion symmetry (with operator $\prod_{j=1}^{N} \sigma_j^x$ being conserved). In our investigation, we focus on the even-Z_2 sector within $\sum_i \langle \sigma_i^z \rangle = 0$ and resolve all the symmetries of the Hamiltonian [21]. The length of chain we consider here is up to $N = 20$, where the dimension of the Hilbert space of the considered sector is $D = N!/[(N/2)!]^2/2 = 92378$.

III. INTEGRABLE-CHAOTIC-NONERGODIC CROSSOVERS DRIVEN BY SPATIAL INHOMOGENEITY OF INTERACTIONS

A. Distribution of level spacing

We first investigate the distribution of energy level spacing $P(s)$ with s the spacing between neighboring unfolded levels. The spectral unfolding is performed so that the mean level spacing is unity [66,67], allowing one to extract short-range spectral correlations of many-body systems, such as $P(s)$, in a robust manner [68]. The distribution $P(s)$ exhibits distinct characteristics depending on whether the system is chaotic or integrable.

For an integrable system, the eigenvalues are uncorrelated and crossings between energy levels are not prohibited, which leads to the Poissonian distribution of level spacings, i.e., $P_{\text{P}}(s) = \exp(-s)$ [69–71]. In contrast, the energy levels in a quantum chaotic system are correlated and the crossings are avoided as level repulsion emerges. Consequently, the level statistics follow the Wigner-Dyson distribution according to the random matrix theory [72]. In our model, which preserves the time-reversal invariance, the appropriate symmetry class is the Gaussian orthogonal ensemble (GOE) and the corresponding Wigner surmise reads $P_{\text{WD}}(s) = (\pi s/2) \exp(-\pi s^2/4)$.

The unfolding procedure mentioned above is performed by introducing a cumulative spectral function $N(E) = \sum_n \Theta(E - E_n)$, where Θ represents the unit step function. We fit $N(E)$ with the polynomials up to 12th order. For robustness, we consider 80% of the energy levels in the regions with high density of states.

The level spacing distributions $P(s)$, for several values of the slope θ, are shown in Fig. 2, where we take $N = 18$ and $\Delta = 1$. For the homogeneous case with $\theta = 0$, $P(s)$ matches accurately the Poissonian distribution (depicted by the red dash line). As the inhomogeneity strength increases, $P(s)$ gradually changes and shows an excellent agreement with the Wigner-Dyson distribution (depicted by the blue solid line) at $\theta \sim 0.5$ [Figs. 2(a)–2(d)]. This indicates the presence of level repulsion and onset of applicability of random matrix statistics. As θ continues to increase, $P(s)$ gradually changes back to the Poissonian distribution [Figs. 2(e)–2(h)]. These results suggest that sufficiently strong inhomogeneity ($\theta \simeq 8$) drives the system from quantum chaos back to integrability.

The observed behavior can be readily understood. At $\theta = 0$, the system (1) is integrable. The multiple conserved quantities break the considered D dimensional sector of Hilbert space into smaller subspaces, giving rise to Poissonian level statistics. Introduction of inhomogeneous interactions, $\theta > 0$, breaks the integrability of the Hamiltonian, giving rise to GOE level statistics for θ of the order of unity. In contrast, for $\theta \gg 1$, the z-z coupling term dominates in the Hamiltonian $\hat{H}_{\text{inho}}$ and the hopping term is not sufficiently strong to delocalize the eigenstates in the eigenbasis of σ_i^z operators, giving rise to Poissonian level statistics.

B. Ratio of consecutive level spacing

To understand better the system size dependence of the observed crossovers as well as to pinpoint the roles of Δ and θ, we investigate the level spacing ratio [73,74] that is
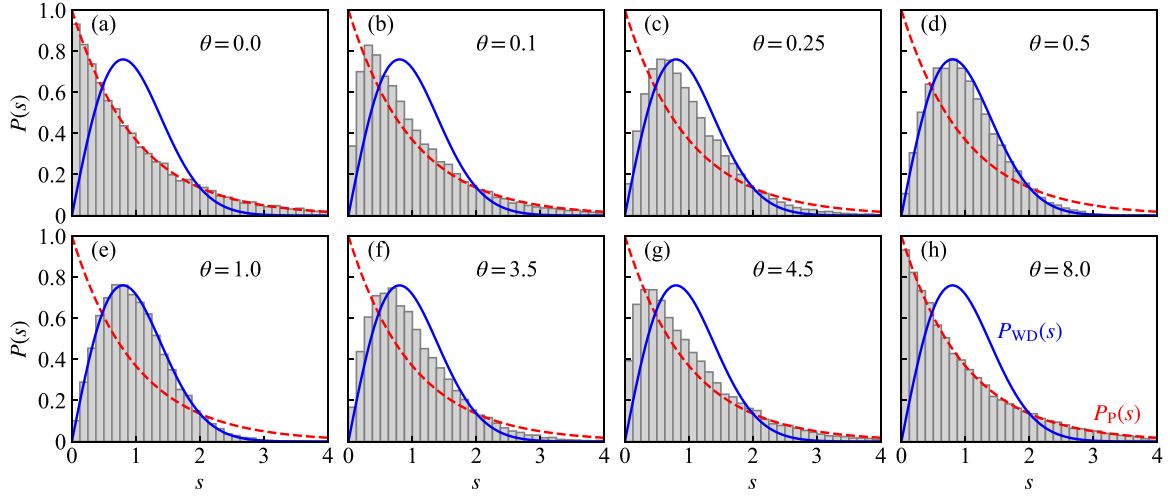
FIG. 2. Level spacing distribution $P(s)$ of the unfolded energy spectra for the inhomogeneous XXZ model [see Eq. (1)]. The red dash and blue solid lines correspond to the Poisson and the Wigner-Dyson distribution, respectively. The results shown are for chains with open boundary conditions and $N = 18$, $\Delta = 1$, even-Z_2 within $\sum_{i=1}^{N}\langle\hat{\sigma}_i^z\rangle = 0$ sector. The 19448 eigenvalues in the middle of the spectrum are used for the calculation.

defined as

$$r = \min\left\{r_n, \frac{1}{r_n}\right\}, \quad r_n = \frac{E_{n+1} - E_n}{E_n - E_{n-1}}, \quad (3)$$

where $\{E_n\}$ are sorted eigenvalues of $\hat{H}_{\text{inho}}$. This ratio serves as another important signature of quantum chaos and it does not require the unfolding procedure.

Its average value $\langle r \rangle$, computed from all eigenenergies, is known to be approximately $\langle r \rangle = r_{\text{GOE}} \simeq 0.5307$ for GOE level statistics and $\langle r \rangle = r_{\text{PS}} \simeq 0.3863$ for Poisson level statistics, respectively.

We begin by studying the integrable to chaotic crossover observed at small values of θ. To that end, we fix $\Delta = 0.5$ and plot $\langle r \rangle$ as a function of θ for system sizes $14 \leqslant N \leqslant 20$, as shown in the top panel of Fig. 3. At each N, we observe that the average level spacing ratio grows from r_{PS} to r_{GOE} with the increase of θ. Notably, this crossover shifts towards smaller values of θ with increasing N, so that the θ_l, i.e., the slope at which the level spacing ratio becomes close to the GOE value $\langle r \rangle = 0.525$, shifts exponentially with N towards smaller values of θ, see the inset in the top panel of Fig. 3. This behavior indicates that in the large system size limit, $N \gg 1$, the system (1) possesses an integrable point at $\theta = 0$ and is quantum chaotic for $0 < \theta < \theta_r$, where θ_r is the inhomogeneity at which the z-z coupling term starts to dominate and the systems become nonergodic.

To probe the latter behavior, we plot $\langle r \rangle$ for larger values of θ and several system sizes N; see the bottom panel of Fig. 3. The interval of θ in which $\langle r \rangle$ is close to GOE (say, bigger than 0.525) extends towards larger and larger values of θ with increasing N. Notably, for $\theta > 5.5$, the $\langle r \rangle(\theta)$ curves for different N approximately collapse on top of each other. This system size dependence of $\langle r \rangle$ is immediately reminiscent of phenomenology observed for the XXZ spin chain with disordered on-site magnetic field [73,75,76]. Understanding of implications of the numerical results for the fate of the disordered system in the thermodynamic limit remains an outstanding challenge in the field of many-body localization (MBL) [77–81]. Indeed, a crossover between $\langle r \rangle = r_{\text{GOE}}$ and
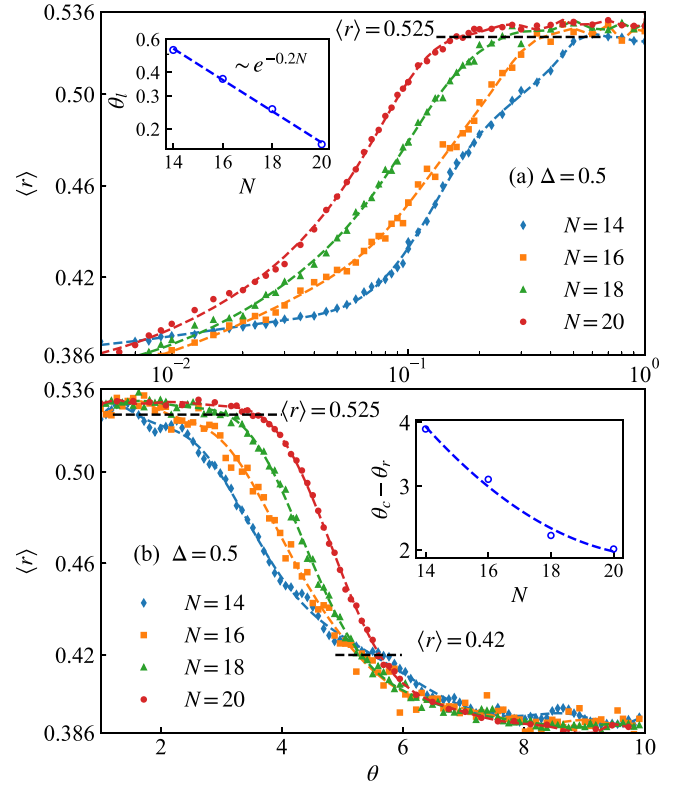

FIG. 3. Average ratio of consecutive level spacings, $\langle r \rangle$, as the function of inhomogeneity θ (a) from 0.01 to 1 and (b) from 1 to 10. We take $\Delta = 0.5$ and $N = 14$, 16, 18, 20. Considering the finite-size effects, the chaotic region (the yellow region in Fig. 4) is identified by $\langle r \rangle > 0.525$. The inset of (a) shows the fitting of the left boundary θ_l of the chaotic region, where we have $\langle r \rangle \simeq 0.525$. The $\theta_c \simeq 5.5$ in (b) is the collapsing point with $\langle r \rangle \simeq 0.42$. The inset of (b) shows the fitting of the right boundary θ_r of the chaotic region. To ensure smoothness in the curve, each blue point for $N = 14$ is given by the average of 10 simulations within its closest range of two neighboring θ values.
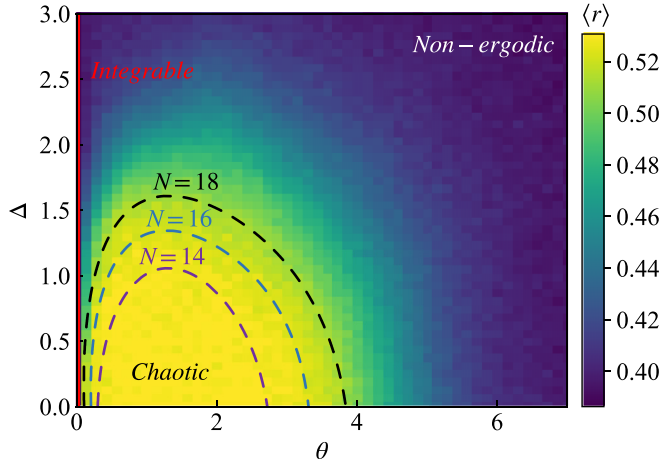
FIG. 4. Average ratio of consecutive level spacings $\langle r \rangle$ for the inhomogeneous *XXZ* chain [Eq. (1)], the system size $N = 18$ with open boundary condition, as a function of the inhomogeneity θ and the average strength Δ. The black (blue, purple) dashed line is the contour of $\langle r \rangle_c \simeq 0.52$ for the system with $N = 18(16, 14)$. The red solid line represents $\theta = 0$, showing the integrable limit of the inhomogeneous *XXZ* chain.

$\langle r \rangle = r_{PS}$ does not necessarily signify ergodicity breaking in the large N limit [82]. One possible scenario for the *XXZ* chain with inhomogeneous interactions consistent with our results is that there exists a finite θ_c (for instance, $\theta_c \approx 5.5$) such that for $\theta < \theta_c$ the system becomes quantum chaotic, $\langle r \rangle \xrightarrow{N \to \infty} r_{GOE}$, while for $\theta > \theta_c$ the system is nonergodic, $\langle r \rangle \xrightarrow{N \to \infty} r_{PS}$. Based on the ED data we cannot, however, exclude other scenarios for the $N \to \infty$ limit. Nevertheless, the observed behavior $\langle r \rangle$ has significant implications for the dynamics of the *XXZ* chain with inhomogeneous interactions at finite times and system sizes. In Sec. V, we demonstrate that the uncovered nonergodic regime has the properties akin to the Stark many-body localization [83–87].

To understand the interplay of Δ and θ we plot $\langle r \rangle$ for $N = 18$ in Fig. 4 on the Δ, θ plane. Note that we only focus on the positive θ and Δ since the plot would be nearly centrosymmetric about the origin ($\theta = 0$ and $\Delta = 0$). For a negative θ, for instance, one can introduce a unitary reflection operation along the chain, which effectively transforms the system back to the positive θ without altering the eigenenergies. For a negative Δ, one can apply $\exp\{\sum_\nu i\frac{\pi}{2}\sigma^z_{2\nu}\}$, a $\pi/2$ rotation along the spin-z direction on the even sites. This operation changes the sign of J while preserving the interactions along z direction. Although this adjustment could introduce a minus sign to the eigenenergies, it does not impact the averaged level spacing ratio according to Eq. (3).

The system is integrable (or nonergodic) when θ is small (or large) enough, as confirmed for various values of Δ in Fig. 4. In the former limit, the system reduces to the typical homogeneous *XXZ* chain. In the latter limit, the system is dominated by the z-z interactions.

When the inhomogeneity θ is comparable to the hopping term, the system is chaotic, which is consistent with the suggestion that, in finite systems, quantum-chaotic properties usually emerge when there are no simplifying descriptions of

the model that would emerge if one of the terms in the Hamiltonian is dominating [36]. Notably, as Δ increases, the range of θ in which the system is chaotic shrinks, indicating the suppression of chaos and thermalization by the z-z interactions. For a sufficiently large Δ, the system is nonergodic for all θ. This behavior is analogous to Hilbert space fragmentation in clean systems [88,89] associated with the strong presence of quasiconservation laws due to strong interactions [90–92] and observed experimentally in the Hubbard model [93,94].

IV. EIGENSTATE THERMALIZATION

In the previous section, we investigated the signatures of quantum chaos, which is one of the consequences of thermalization in the inhomogeneous *XXZ* chain. We will now investigate directly the eigenstate thermalization hypothesis (ETH) by exploring the statistics of the matrix elements of local operators in the eigenstates of (1). The properties of matrix elements of the inhomogeneous interacting *XXZ* chain in the nonergodic regime will be presented for comparison and to enhance our understanding of the latter regime [43,95].

The ETH ansatz for the matrix element of an observable, denoted as $O_{nm} = \langle n|O|m \rangle$ in energy eigenstates (with $\hat{H}|m\rangle = E_m|m\rangle$), can be written as

$$O_{nm} = O(\bar{E})\delta_{nm} + e^{-S(\bar{E})/2} f_O(\bar{E}, \omega) R_{nm}, \qquad (4)$$

with $\bar{E} = (E_n + E_m)/2$ and $\omega = E_m - E_n$. Here, $S(\bar{E})$ denotes the thermodynamic entropy at the energy $\bar{E}$ equal to the logarithm of the density of states [96]; $O(\bar{E})$ and $f_O(\bar{E}, \omega)$ are smooth functions; R_{nm} is a Gaussian-distributed variable with zero mean and unit variance.

The first term in Eq. (4) ensures that when the energy fluctuations in the initial state are subextensive, the equilibrated result can be described using statistical mechanical ensembles. The factor $e^{-S(\bar{E})/2}$ in the second term suggests that the off-diagonal matrix elements decrease exponentially with system size. Up to random fluctuations, these elements are characterized by a smooth function $f_O(\bar{E}, \omega)$ [21,29,33,36,43,97] that carries crucial information on the quantum thermalization and fluctuation dissipation relations [21,29,38,98–102]. It is worth noting that R_{nm} is similar to the random matrices in the GOE. However, the higher-order correlations are not described by GOE or the random matrix theory [45,100,103–106]. Here, our primary target is to probe the nature of the distribution of matrix elements, while the higher-order statistical correlations remain beyond the scope of this work.

We consider the matrix elements of two operators, $\hat{T}$ and $\hat{Z}$. $\hat{T}$ is the next-nearest-neighboring "kinetic" energy per site

$$\hat{T} = \frac{1}{N} \sum_{i=1}^{N-2} \left(\sigma^x_i \sigma^x_{i+2} + \sigma^y_i \sigma^y_{i+2} \right). \qquad (5)$$

$\hat{Z}$ contains the nearest-neighboring z-z interactions with a spatially inhomogeneous coefficient, which is defined as

$$\hat{Z} = \frac{1}{N} \sum_{i=1}^{N-1} \tilde{\Delta}_i \hat{\sigma}^z_i \hat{\sigma}^z_{i+1}. \qquad (6)$$
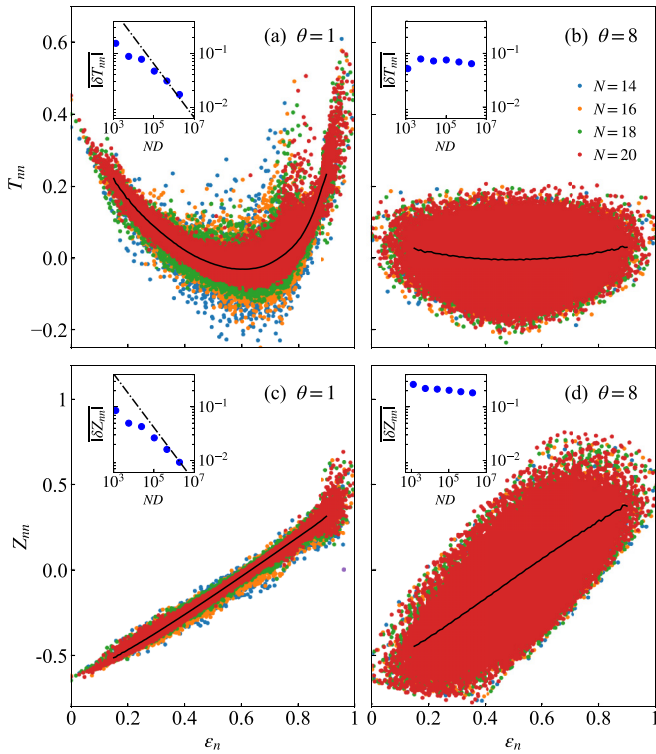
FIG. 5. Diagonal matrix elements of $\hat{T}$ [(a), (b)] and $\hat{Z}$ [(c), (d)] in the eigenstates of $\hat{H}_{\text{Inho}}$ in the quantum chaotic regime ($\Delta = 1$, $\theta = 1$) [(a), (c)] and in the nonergodic regime ($\Delta = 1$, $\theta = 8$) [(b), (d)]. The black lines represent the microcanonical averages (within windows of $\delta\varepsilon_n = 0.01$) for the largest chain size ($N = 20$). The insets exhibit the scaling behavior of $\overline{|\delta O_{nn}|} = \overline{|O_{nn} - O_{n+1n+1}|}$ (for $O = T, Z$) with respect to ND [the dashed lines indicate the line $\propto (ND)^{-1/2}$]. The averaging is performed over the central 20% of the eigenstates in the Hamiltonian described by Eq. (1) with N from 10 to 20.

The coefficient $\tilde{\Delta}_i$ takes the same expression as Eq. (2) with $\Delta = 1$ and $\theta = 1$. We expect that the specific choices of operators do not affect our main conclusions.

A. Diagonal matrix elements

Figures 5(a), 5(b) and 5(c), 5(d) show the diagonal matrix elements $T_{nn} = \langle n|\hat{T}|n\rangle$ and $Z_{nn} = \langle n|\hat{Z}|n\rangle$, respectively. These results are obtained in the even-Z_2 sector within the $\sum_i \langle \sigma_i^z \rangle = 0$ sector (see Sec. II). The matrix elements are plotted as functions of the energy density, defined as $\varepsilon_n = (E_n - E_{\min})/(E_{\max} - E_{\min})$, where E_n represents the nth eigenvalue of (1), while $E_{\max}$ and $E_{\min}$ are the highest and lowest eigenvalues.

In the quantum chaotic regime, at $\Delta = \theta = 1$, we observe a decrease of the support of both T_{nn} and Z_{nn} around the ε_n away from the edges of the spectrum as the system size N increases [see Figs. 5(a) and 5(c)]. Meanwhile, an exponential decay of the average strength of the eigenstate-to-eigenstate fluctuations, $\overline{|\delta T_{nn}|}$ [34,36,43,47,107,108], is shown in the insets of Fig. 5(a). Similar observations are shown in the inset of Fig. 5(c) for δZ_{nn}. Thus the diagonal matrix elements, up to the exponentially decaying fluctuations, follow a smooth function

of energy which agrees with the microcanonical predictions of these observables as shown by the black solid lines in the main panels of 5(a) and 5(c). These results are also consistent with the ETH, regardless of whether the observable is homogeneous ($\hat{T}$) or not ($\hat{Z}$).

In the nonergodic regime, at $\Delta = 1, \theta = 8$ [see Figs. 5(b) and 5(d)], we observe that the support of distributions of T_{nn} and Z_{nn} remains wide and does not shrink with the system size N. The insets also show that the eigenstate-to-eigenstate fluctuations exhibit a very slow or even no decay as N increases. This wide and nonshrinking support indicates the absence of diagonal eigenstate thermalization for these observables in the nonergodic inhomogeneous *XXZ* chain. This observation is consistent with Poissonian level statistics of the system and shows that the model violates the ETH.

B. Off-diagonal matrix elements

We now turn to the off-diagonal matrix elements of observables $T_{nm} \equiv \langle n|\hat{T}|m\rangle$ and $Z_{nm} \equiv \langle n|\hat{Z}|m\rangle$ in the energy eigenbasis and focus on the second term of the ETH ansatz [Eq. (4)]. Since $\hat{T}$ and $\hat{Z}$ are averaged local operators, the ETH ansatz for the off-diagonal matrix elements of a single local operator should be modified to [43,47,109,110]

$$O_{nm} = \frac{e^{-S(\bar{E})/2}}{\sqrt{N}} f_O(\bar{E}, \omega) R_{nm}. \qquad (7)$$

We focus on the region with $\bar{E} \simeq 0$, which corresponds to the "infinite-temperature" region as $S(\bar{E}) \simeq \ln D$.

Figure 6 illustrates the distribution of the off-diagonal matrix elements $|T_{nm}|^2$ and $|Z_{nm}|^2$ using normalized 2D histograms, along with the coarse-grained averages $\overline{|T_{nm}|^2}$ and $\overline{|Z_{nm}|^2}$ as a function of ω. These averages correspond to the variances of the off-diagonal matrix elements as $\overline{T_{nm}} = \overline{Z_{nm}} = 0$. In the chaotic regime ($\Delta = \theta = 1$), the variances change smoothly with ω [43,47] [see Figs. 6(a) and 6(c)]. Both the homogeneous observable $\hat{T}$ and inhomogeneous $\hat{Z}$ exhibit a slow decay at the intermediate values of ω and a relative rapid decay at larger ω. Nearly perfect collapses of variances for different system sizes are demonstrated, indicating that the variances of the off-diagonal matrix elements satisfy $\overline{|O_{nm}|^2} \propto (N\mathcal{D})^{-1}$ for $O = T, Z$. These results are in full agreement with the ETH [21,43,45,47].

For our inhomogeneous *XXZ* chain in the nonergodic regime, Figs. 6(b) and 6(d) show the distributions of the off-diagonal matrix elements and their coarse-grained averages. Remarkable differences are observed in comparison to the chaotic region. First, the overall dispersion is much larger than that at the quantum-chaotic points, consistent with the previous results [43,47]. Second, the coarse-grained averages ($\overline{|O_{nm}|^2}$) at a nonergodic point do not evidently show the trend to drop as ω increases and change nonsmoothly with ω. Thirdly, we find no data collapsing for different system sizes N. These differences between integrability and chaos in our inhomogeneous system are inconsistent with the ETH. Note that, for the conventional homogeneous integrable *XXZ* model, the off-diagonal matrix element variances behave smoothly and the data collapse
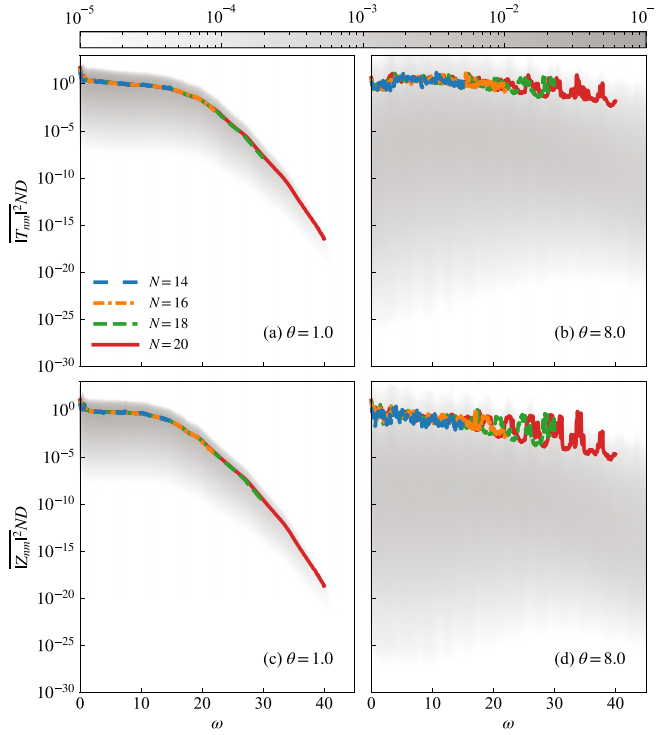
FIG. 6. Normalized 2D histograms of the off-diagonal matrix elements and the corresponding coarse-grained average of $\hat{T}$ [(a), (b)] and $\hat{Z}$ [(c), (d)] for different chain sizes as a function of ω. Panels (a), (c) correspond to the nonintegrable point of the inhomogeneous *XXZ* model with parameters $\Delta = 1$, $\theta = 1$, while panels (b), (d) present results for the nonergodic point with $\Delta = 1$, $\theta = 8$. The matrix elements were computed within a small energy window around $\bar{E} \simeq 0$, the center of the spectrum, with a width of 0.075ε, where $\varepsilon = E_{\max} - E_{\min}$. The coarse-grained averages in ω were calculated using windows of width $\delta\omega = 0.1$.

for different system sizes, which are similar to its chaotic counterpart [43,44,46,47].

To test the normality of the distribution of the off-diagonal matrix elements, we evaluate the frequency-dependent ratio

$$\Gamma_{\hat{O}}(\omega) = \overline{|O_{nm}|^2} / \overline{|O_{nm}|}^2. \tag{8}$$

This ratio is equal to $\pi/2$ when O_{nm} obeys the Gaussian distribution with zero mean [43]. Figure 7 illustrates $\Gamma_{\hat{T}}(\omega)$ and $\Gamma_{\hat{Z}}(\omega)$ for the inhomogeneous *XXZ* chain. In the chaotic regime [$\theta = 1$; see Figs. 7(a) and 7(c)], the ratios are close to $\pi/2$ at the intermediate frequencies and deviate from $\pi/2$ for lower and higher frequencies. The deviations are caused by the finite-size effects and are suppressed by increasing the system size N. The presented results indicate that the distribution of the off-diagonal matrix elements T_{nm} and Z_{nm} is the Gaussian distribution in a wide frequency range for sufficiently large N, consistently with the prediction of ETH.

In contrast, the behaviors of the ratios for the nonergodic inhomogeneous chain ($\theta = 8$) are strongly affected by the system size N [see Figs. 7(b) and 7(d)]. The value deviates further from $\pi/2$ as N increases, indicating that the distribution of off-diagonal matrix elements T_{nm} and Z_{nm} is not Gaussian.
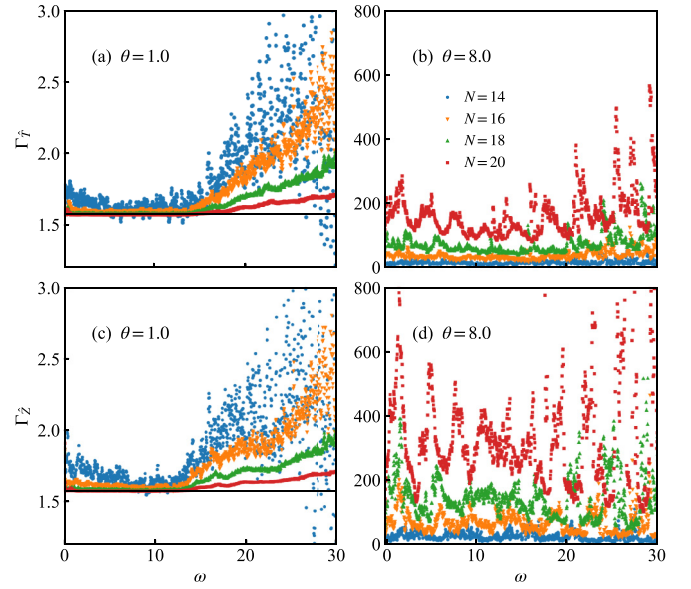

FIG. 7. $\Gamma_{\hat{O}}(\omega)$ [see Eq. (8)] for $\hat{T}$ [(a), (b)] and for $\hat{Z}$ [(c), (d)] in the nonintegrable inhomogeneous *XXZ* chain with $\Delta = 1$, $\theta = 1$ [(a), (c)] and the nonergodic one with $\Delta = 1$, $\theta = 8$ [(b), (d)]. In (a) and (c), the horizontal line denotes $\pi/2$. The matrix elements were computed within a narrow energy window of width 0.075ε, where $\varepsilon = E_{\max} - E_{\min}$. The coarse-grained averages were calculated using a window size of $\delta\omega = 0.1$.

The distributions of off-diagonal matrix elements near zero frequency are depicted in Fig. 8. In the chaotic regime [$\theta = 1$, panels (a) and (c)], the reliability of ETH is confirmed by the remarkable agreement with the Gaussian distribution. Additionally, comparing the case of $\Delta = 0$ with $\Delta = 1$ (see the insets), we find that the agreement with Gaussian distribution is better for $\Delta = 0$. Nevertheless, both distributions tend towards a Gaussian distribution as the system size increases, as supported by Fig. 7. In the nonergodic regime [$\theta = 8$, panels (b) and (d)], the $\ln |O_{nm}|$ distribution has a skewed normal-like shape as typically observed in the integrable *XXZ* model [43], even though the overall frequency behavior depicted in Fig. 6 is different.

V. DYNAMICS

The results shown above concern the matrix elements of local operators, which demonstrate the ETH behavior of the inhomogeneous *XXZ* spin chain. In this section, we explore the thermalization and ergodicity breaking in the system by investigating time evolution of the entanglement entropy and the survival probability, of which both are relevant to the quench experiments with quantum simulators.

A. Entanglement entropy

We first investigate the time evolution of the entanglement entropy for a bipartition of the chain into two halves. The entanglement entropy at the time t is defined as

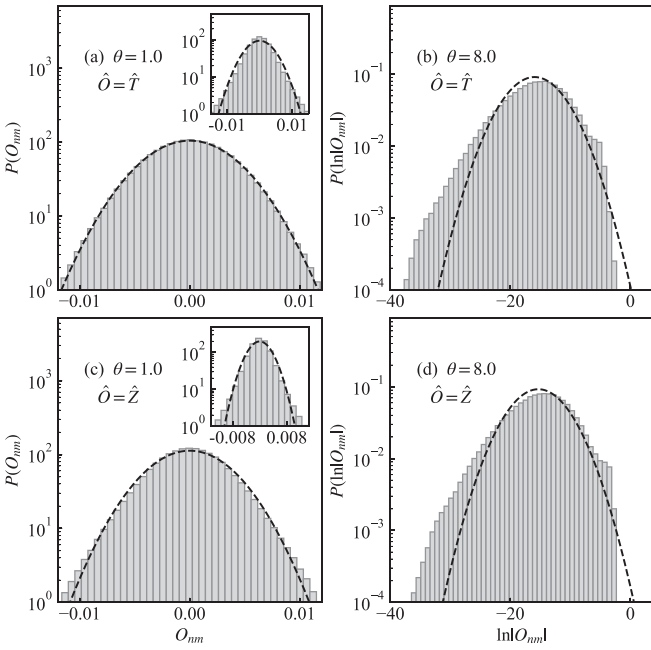$$S(t) = -\operatorname{Tr}\left[\hat{\rho}_R(t) \ln \hat{\rho}_R(t)\right], \tag{9}$$

FIG. 8. Probability distributions $P(O_{nm})$ for observables $\hat{T}$ and $\hat{Z}$ [(a), (c)] for quantum chaotic Hamiltonian with $\theta = 1$, $\Delta = 0$ ($\theta = 1$, $\Delta = 1$) in the main panel (inset), along with Gaussian distributions (dash lines) with the same mean and variance. We consider the eigenpairs around $\bar{E} \approx 0$ within a narrow energy window of width 0.075ε, where $\varepsilon = E_{max} - E_{min}$, and $\omega < 0.1$. The probability distributions $P(\ln |O_{nm}|)$ of the matrix elements of $\hat{T}$ and $\hat{Z}$, respectively, along with the log-normal distributions (dash line), are shown in panels (b) and (d) for the nonergodic Hamiltonian with $\theta = 8$ and $\Delta = 0$.

where $\rho_R(t)$ represents the reduced density matrix at the time t after tracing over the degrees of freedom residing in one of the halves of the chain. Here, as the initial states, we consider the product states, where the spin on each site is drawn randomly to be oriented either up or down in the z direction.

The behavior of $S(t)$ for different choices of Δ and θ is illustrated in Fig. 9. The results are averaged over 10^3 time evolutions with different initial product states. In (a), we show the $S(t)$ in the chaotic region ($\Delta = 0$ and $\theta = 1$) for various system sizes ranging from $N = 8$ to 16. There is an early-time ballistic linear growth of $S(t)$ that persists to longer times with increasing N [111]. Subsequently, the growth of $S(t)$ eventually saturates at the Page value $S = N/2 \ln 2 - 1/2$ [112] up to an $O(1)$ correction associated with the symmetry of $\hat{H}_{inho}$ [113,114]. These results indicate the ergodic dynamics, implying the occurrence of thermalization.

In Fig. 9(b), we compare the ergodic dynamics observed for $\Delta = 0$, $\theta = 1$ with the nonergodic dynamics that arise at large θ. In the nonergodic regime, at $\Delta = 0$, $\theta = 8$, the entanglement entropy exhibits logarithmic growth at long times, $S(t) \sim \ln(t)$. This logarithmic behavior of $S(t)$ in our inhomogeneous nonergodic XXZ spin chain resembles the observations in the MBL systems, where $S(t)$ grows logarithmically with time [115–119]. Interestingly, increasing either θ in the inhomogeneous XXZ chain or Δ in the homogeneous chain would have a similar effect which, in the case of MBL systems, stems from the presence of localized integrals of motion [120–123]. This observation suggests po-
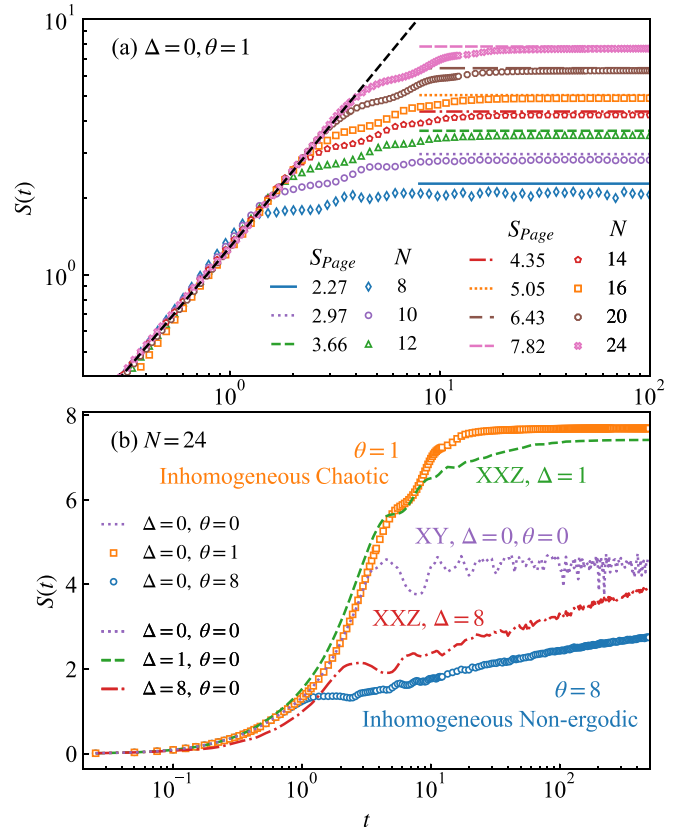
FIG. 9. (a) Evolution of entanglement entropy $S(t)$ in the chaotic region ($\Delta = 0$ and $\theta = 1$) with different system sizes N. The black dashed line represents the fitting at short times [$t\,O(10^0)$]. The asymptotic saturation values of $S(t)$ for large t are indicated by the Page values (see the horizontal dashed lines). (b) The $S(t)$ in the system with various Δ's and θ's. See the analyses in the main text. Note each data point in this figure is the average over the simulations from about 10^3 distinct initial states.

tential connections between the phenomenology of MBL and the dynamics of systems with shattered Hilbert space due to significant z-z interactions.

B. Survival probability

To further probe the dynamics of the XXZ spin chain with inhomogeneous interactions and to highlight the memory effects occurring in the nonergodic regime, we consider the survival probability of the initial state is defined as

$$P(t) = |\langle \psi(0)|e^{-i\hat{H}_{inho}t}|\psi(0)\rangle|^2, \qquad (10)$$

where $\psi(0)$ is the initial state and $e^{-i\hat{H}_{inho}t}$ is the time evolution operator for our system. Alternatively, the survival probability can also be expressed as the norm square of the Fourier transformation of the local density of state (LDOS), obeying

$$P(t) = \left| \int dE\, \rho(E) e^{-iEt} \right|^2, \qquad (11)$$

where the LDOS is given by $\rho(E) = \sum_n |C_n|^2 \delta(E - E_n)$ [with $C_n = \langle E_n|\psi(0)\rangle$ and $|E_n\rangle$ the nth eigenstate of $\hat{H}_{inho}$]. Figure 10 shows the survival probability $P(t)$ averaged over
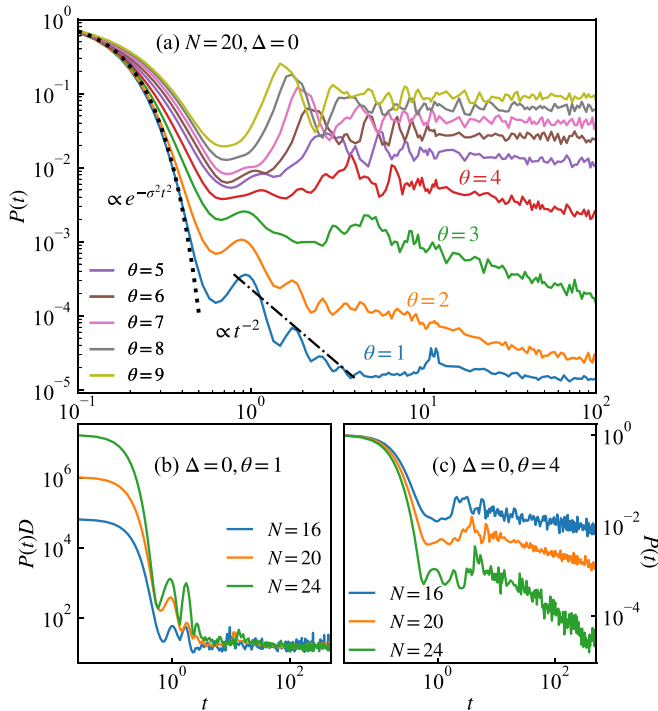
FIG. 10. (a) Decay of the survival probability $P(t)$ for various θ with $\Delta = 0$ and $N = 20$. The dotted line illustrates a Gaussian decay with σ (the variance of the LDOS with $\theta = 1$). The dash-dotted line is proportional to t^{-2}. Each curve is given by the average over 10^3 different initial states. (b) Survival probability multiplied by Hilbert space dimension, $P(t)D$, as function of time in the ETH regime, $\Delta = 0$, $\theta = 1$. (c) Persistent decay of the survival probability $P(t)$ at the crossover between ETH and nonergodic regions.

10^3 initial random product states polarized in z direction for different values of θ ranging from 1 to 9, with fixed $\Delta = 0$.

In the chaotic region [see as illustrated by the results for $\theta = 1$–3 in Fig. 10(a)], the decay is Gaussian for the early time [124–127]. This suggests that the LDOS is Gaussian-shaped, i.e., the coefficients C_n do not add any specific structure on top of the Gaussian density of states at large energy scales. Subsequently, the decay of $P(t)$ changes to a power law and eventually saturates at a value that is exponentially small in the systems size N [128,129], as shown in Fig. 10(b). This behavior signals occurrence of thermalization in the system.

With increasing inhomogeneity strength θ, we observe a significant slowdown of the decay of the survival probability. Upon entering into the nonergodic, nonergodic region, for $\theta > 4$, we observe only a residual power-law decay of $P(t)$ with the exponent that decreases rapidly with θ. We have checked that the survival probability at large times is decreasing slower than exponentially quickly with system size in this regime (data not shown). While our results in the nonergodic region of the inhomogeneous *XXZ* spin chain demonstrate the memory of the initial state at the considered system sizes N and time scales t, our numerical data are insufficient to decide whether this behavior persists in the asymptotic limit of large t and N. The decay of survival probability is slow, but the decreasing of $P(t)$ tends to be faster with increasing N even at the largest values of θ considered here. This behavior is especially well

pronounced in the region intermediate between the ETH and nonergodic regimes, as illustrated in Fig. 10(c).

The uncovered features of time evolution in the *XXZ* spin chain with inhomogeneous interactions are similar to the behavior of strongly disordered many-body systems [130,131] ultimately preventing us from distinguishing a regime of very slow thermalization from ergodicity breaking phenomenon in the asymptotic limit $t \to \infty$, $N \to \infty$ [132].

VI. EXPERIMENTAL IMPLEMENTATION

The experimental realization of the *XXZ* model presented in Eq. (1) can benefit from recent advances in atomic systems and waveguide QED. In particular, the spin degree of freedom is mapped to two metastable states of the atoms, whose position can be optically controlled with the use of optical lattices or atomic tweezers. Spin exchange naturally appears when atomic dipolar interactions are strong enough to compete with the finite lifetime (τ) of their internal levels ($J\tau \gg 1$). This is the case of magnetic atoms in short optical lattices, where single atom addressing becomes challenging due to the diffraction limit and new strategies are being put into place [133]. Another emergent platform consists of atoms coupled to waveguides, where spin exchange can be mediated by exponentially localized photons emitted into the fiber, and additional control fields can be used to engineer the desired *XXZ* interactions [134]. In this open-quantum system, other additional terms not conserving the number of excitations would enter as well, though [135].

An alternative consists of using Rydberg atoms, where the strength of dipolar interactions scales with the quantum number n of the valence electron as n^4, leading to strong forces even for typical atomic separations of $r \sim 1$ μm. While the resulting spin-exchange terms are of the form *XX*, the *XXZ* Hamiltonian can be engineered in a Floquet manner by appropriately rotating the spin axis at regular time intervals, as it has been experimentally realized in [133]. Single-atom addressing can then be used to modulate the desired linear tilt Δ_i in the $\sigma_i^z \sigma_{i+1}^z$ term of each atom in the array in the regime $0 \leqslant \Delta \pm \theta \leqslant 2J$, where both the chaotic and nonergodic regimes can be accessed. Using randomized measurements one can extract arbitrary observables [136], including the entanglement entropy of the chain [137]. Following this approach, dipolar interactions decay polynomially as r^{-3} and the role of next-nearest-neighbor interactions (which are one order of magnitude weaker than the nearest-neighbor ones) will be the subject of future work.

VII. SUMMARY AND PERSPECTIVE

Our work extends the explorations of the interplay of ETH and quantum chaos with ergodicity breaking to the systems with linearly inhomogeneous interactions. We demonstrate that insertion of a suitable inhomogeneity of the *z-z* interactions leads to the onset of quantum chaos in the spin-1/2 *XXZ* chain, while a sufficiently large inhomogeneity restores the integrability of the system. While our results hold for a clean system, similar phenomenology can be found also in systems with disordered interactions; see [138–141].

To support our conclusions, we probe level statistics of the inhomogeneous *XXZ* spin chain and study statistical properties of matrix elements of local observables in eigenstates of the system. In the quantum chaotic regime, the support and average eigenstate-to-eigenstate fluctuations of the diagonal elements vanish exponentially with the system size. Furthermore, the off-diagonal elements follow a Gaussian distribution and their variances exhibit a well-defined smooth function $|f_O(\bar{E} \simeq 0, \omega)|^2$ with respect to the frequency ω. These results are fully consistent with the ETH. In contrast, the system exhibits essentially different behavior in the nonergodic regions with strong inhomogeneity. The variances of off-diagonal matrix elements are not anymore the smooth function of energy. Notably, the observed behavior is also different from other integrable models such as the homogeneous *XXZ* chain.

We also investigate the dynamics of the entanglement entropy and survival probability, both of which can be probed in quench experiments with quantum simulators. In the chaotic region, we find a ballistic spreading of entanglement entropy and an abrupt decay of the survival probability. These results indicate the ergodic dynamics, implying the occurrence of thermalization. Conversely, in the nonergodic region with the large inhomogeneity, entropy exhibits logarithmic growth and the survival probability remains significant even at longer times, indicating the presence of the memory in the system. This closely resembles the observations for the strongly disordered MBL phase and stems from Hilbert space shattering due to strong interactions in the system.

ACKNOWLEDGMENTS

[1] J. V. Neumann, Beweis des Ergodensatzes und des H-Theorems in der neuen Mechanik, Z. Phys. **57**, 30 (1929).

[2] S. Goldstein, J. L. Lebowitz, R. Tumulka, and N. Zanghì, Long-time behavior of macroscopic quantum systems. Commentary accompanying the English translation of John von Neumann's 1929 article on the quantum ergodic theorem, Eur. Phys. J. H **35**, 173 (2010).

[3] I. Bloch, J. Dalibard, and W. Zwerger, Many-body physics with ultracold gases, Rev. Mod. Phys. **80**, 885 (2008).

[4] T. Langen, R. Geiger, and J. Schmiedmayer, Ultracold atoms out of equilibrium, Annu. Rev. Condens. Matter Phys. **6**, 201 (2015).

[5] J. Eisert, M. Friesdorf, and C. Gogolin, Quantum many-body systems out of equilibrium, Nat. Phys. **11**, 124 (2015).

[6] M. Lewenstein, A. Sanpera, V. Ahufinger, B. Damski, A. Sen, and U. Sen, Ultracold atomic gases in optical lattices: mimicking condensed matter physics and beyond, Adv. Phys. **56**, 243 (2007).

[7] I. Bloch, J. Dalibard, and S. Nascimbène, Quantum simulations with ultracold quantum gases, Nat. Phys. **8**, 267 (2012).

[8] S. Trotzky, Y. A. Chen, A. Flesch, I. P. McCulloch, U. Schollwöck, J. Eisert, and I. Bloch, Probing the relaxation towards equilibrium in an isolated strongly correlated one-dimensional Bose gas, Nat. Phys. **8**, 325 (2012).

[9] A. M. Kaufman, M. E. Tai, A. Lukin, M. Rispoli, R. Schittko, P. M. Preiss, and M. Greiner, Quantum thermalization through entanglement in an isolated many-body system, Science **353**, 794 (2016).

[10] C. Neill, P. Roushan, M. Fang, Y. Chen, M. Kolodrubetz, Z. Chen, A. Megrant, R. Barends, B. Campbell, B. Chiaro, A. Dunsworth, E. Jeffrey, J. Kelly, J. Mutus, P. J. J. O'Malley, C. Quintana, D. Sank, A. Vainsencher, J. Wenner, T. C. White *et al.*, Ergodic dynamics and thermalization in an isolated quantum system, Nat. Phys. **12**, 1037 (2016).

[11] Y. Tang, W. Kao, K.-Y. Li, S. Seo, K. Mallayya, M. Rigol, S. Gopalakrishnan, and B. L. Lev, Thermalization near

integrability in a dipolar quantum newton's cradle, Phys. Rev. X **8**, 021030 (2018).

[12] G. Clos, D. Porras, U. Warring, and T. Schaetz, Time-resolved observation of thermalization in an isolated quantum system, Phys. Rev. Lett. **117**, 170401 (2016).

[13] T. Kinoshita, T. Wenger, and D. S. Weiss, A quantum Newton's cradle, Nature (London) **440**, 900 (2006).

[14] M. Gring, M. Kuhnert, T. Langen, T. Kitagawa, B. Rauer, M. Schreitl, I. Mazets, D. A. Smith, E. Demler, and J. Schmiedmayer, Relaxation and prethermalization in an isolated quantum system, Science **337**, 1318 (2012).

[15] T. Langen, S. Erne, R. Geiger, B. Rauer, T. Schweigler, M. Kuhnert, W. Rohringer, I. E. Mazets, T. Gasenzer, and J. Schmiedmayer, Experimental observation of a generalized Gibbs ensemble, Science **348**, 207 (2015).

[16] L. Vidmar and M. Rigol, Generalized gibbs ensemble in integrable lattice models, J. Stat. Mech.: Theory Exp. (2016) 064007.

[17] J. M. Deutsch, Quantum statistical mechanics in a closed system, Phys. Rev. A **43**, 2046 (1991).

[18] M. Srednicki, Chaos and quantum thermalization, Phys. Rev. E **50**, 888 (1994).

[19] M. Rigol, V. Dunjko, and M. Olshanii, Thermalization and its mechanism for generic isolated quantum systems, Nature (London) **452**, 854 (2008).

[20] S. Pappalardi, L. Foini, and J. Kurchan, Microcanonical windows on quantum operators, Quantum **8**, 1227 (2024).

[21] L. D'Alessio, Y. Kafri, A. Polkovnikov, and M. Rigol, From quantum chaos and eigenstate thermalization to statistical mechanics and thermodynamics, Adv. Phys. **65**, 239 (2016).

[22] C. Dankert, R. Cleve, J. Emerson, and E. Livine, Exact and approximate unitary 2-designs and their application to fidelity estimation, Phys. Rev. A **80**, 012304 (2009).

[23] D. Voiculescu, Limit laws for random matrices and free products, Invent. Math. **104**, 201 (1991).

[24] S. Pappalardi, L. Foini, and J. Kurchan, Eigenstate thermalization hypothesis and free probability, Phys. Rev. Lett. **129**, 170603 (2022).

[25] S. Pappalardi, F. Fritzsch, and T. Prosen, General eigenstate thermalization via free cumulants in quantum lattice systems, arXiv:2303.00713 [cond-mat.stat-mech].

[26] M. Fava, J. Kurchan, and S. Pappalardi, Designs via free probability, arXiv:2308.06200 [quant-ph].

[27] M. Rigol, Breakdown of thermalization in finite one-dimensional systems, Phys. Rev. Lett. **103**, 100403 (2009).

[28] R. Steinigeweg, J. Herbrych, and P. Prelovšek, Eigenstate thermalization within isolated spin-chain systems, Phys. Rev. E **87**, 012118 (2013).

[29] E. Khatami, G. Pupillo, M. Srednicki, and M. Rigol, Fluctuation-dissipation theorem in an isolated system of quantum dipolar bosons after a quench, Phys. Rev. Lett. **111**, 050403 (2013).

[30] W. Beugeling, R. Moessner, and M. Haque, Finite-size scaling of eigenstate thermalization, Phys. Rev. E **89**, 042112 (2014).

[31] S. Sorg, L. Vidmar, L. Pollet, and F. Heidrich-Meisner, Relaxation and thermalization in the one-dimensional bose-hubbard model: A case study for the interaction quantum quench from the atomic limit, Phys. Rev. A **90**, 033606 (2014).

[32] R. Steinigeweg, A. Khodja, H. Niemeyer, C. Gogolin, and J. Gemmer, Pushing the limits of the eigenstate thermalization hypothesis towards mesoscopic quantum systems, Phys. Rev. Lett. **112**, 130403 (2014).

[33] W. Beugeling, R. Moessner, and M. Haque, Off-diagonal matrix elements of local operators in many-body quantum systems, Phys. Rev. E **91**, 012144 (2015).

[34] R. Mondaini, K. R. Fratus, M. Srednicki, and M. Rigol, Eigenstate thermalization in the two-dimensional transverse field ising model, Phys. Rev. E **93**, 032104 (2016).

[35] T. Yoshizawa, E. Iyoda, and T. Sagawa, Numerical large deviation analysis of the eigenstate thermalization hypothesis, Phys. Rev. Lett. **120**, 200604 (2018).

[36] D. Jansen, J. Stolpp, L. Vidmar, and F. Heidrich-Meisner, Eigenstate thermalization and quantum chaos in the holstein polaron model, Phys. Rev. B **99**, 155130 (2019).

[37] I. M. Khaymovich, M. Haque, and P. A. McClarty, Eigenstate thermalization, random matrix theory, and behemoths, Phys. Rev. Lett. **122**, 070601 (2019).

[38] C. Schönle, D. Jansen, F. Heidrich-Meisner, and L. Vidmar, Eigenstate thermalization hypothesis through the lens of autocorrelation functions, Phys. Rev. B **103**, 235137 (2021).

[39] J. D. Noh, Eigenstate thermalization hypothesis in two-dimensional *xxz* model with or without su(2) symmetry, Phys. Rev. E **107**, 014130 (2023).

[40] T. D. Anh-Tai, M. Mikkelsen, T. Busch, and T. Fogarty, Quantum chaos in interacting Bose-Bose mixtures, SciPost Phys. **15**, 048 (2023).

[41] O. S. Barišić, P. Prelovšek, A. Metavitsiadis, and X. Zotos, Incoherent transport induced by a single static impurity in a heisenberg chain, Phys. Rev. B **80**, 125118 (2009).

[42] M. Brenes, E. Mascarenhas, M. Rigol, and J. Goold, High-temperature coherent transport in the xxz chain in the presence of an impurity, Phys. Rev. B **98**, 235128 (2018).

[43] T. LeBlond, K. Mallayya, L. Vidmar, and M. Rigol, Entanglement and matrix elements of observables in interacting integrable systems, Phys. Rev. E **100**, 062134 (2019).

[44] T. LeBlond and M. Rigol, Eigenstate thermalization for observables that break hamiltonian symmetries and its counterpart in interacting integrable systems, Phys. Rev. E **102**, 062113 (2020).

[45] J. Richter, A. Dymarsky, R. Steinigeweg, and J. Gemmer, Eigenstate thermalization hypothesis beyond standard indicators: Emergence of random-matrix behavior at small frequencies, Phys. Rev. E **102**, 042127 (2020).

[46] M. Brenes, J. Goold, and M. Rigol, Low-frequency behavior of off-diagonal matrix elements in the integrable xxz chain and in a locally perturbed quantum-chaotic xxz chain, Phys. Rev. B **102**, 075127 (2020).

[47] M. Brenes, T. LeBlond, J. Goold, and M. Rigol, Eigenstate thermalization in a locally perturbed integrable system, Phys. Rev. Lett. **125**, 070605 (2020).

[48] R. Vasseur, J. P. Dahlhaus, and J. E. Moore, Universal nonequilibrium signatures of majorana zero modes in quench dynamics, Phys. Rev. X **4**, 041007 (2014).

[49] J. Viti, J.-M. Stéphan, J. Dubail, and M. Haque, Inhomogeneous quenches in a free fermionic chain: Exact results, Europhys. Lett. **115**, 40011 (2016).

[50] N. Allegra, J. Dubail, J.-M. Stéphan, and J. Viti, Inhomogeneous field theory inside the arctic circle, J. Stat. Mech.: Theory Exp. (2016) 053108.

[51] J. Dubail, J.-M. Stéphan, J. Viti, and P. Calabrese, Conformal field theory for inhomogeneous one-dimensional quantum systems: the example of non-interacting Fermi gases, SciPost Phys. **2**, 002 (2017).

[52] N. Bondyopadhaya and D. Roy, Dynamics of hybrid junctions of majorana wires, Phys. Rev. B **99**, 214514 (2019).

[53] A. Biella, M. Collura, D. Rossini, A. De Luca, and L. Mazza, Ballistic transport and boundary resistances in inhomogeneous quantum spin chains, Nat. Commun. **10**, 4820 (2019).

[54] K. Gawędzki and K. K. Kozłowski, Full counting statistics of energy transfers in inhomogeneous nonequilibrium states of (1 +1)D CFT, Commun. Math. Phys. **377**, 1227 (2020).

[55] G. del Vecchio del Vecchio, A. De Luca, and A. Bastianello, Transport through interacting defects and lack of thermalisation, SciPost Phys. **12**, 060 (2022).

[56] M. Ljubotina, D. Roy, and T. Prosen, Absence of thermalization of free systems coupled to gapped interacting reservoirs, Phys. Rev. B **106**, 054314 (2022).

[57] D.-Z. Wang, G.-F. Zhang, M. Lewenstein, and S.-J. Ran, Boundary-induced singularity in strongly-correlated quantum systems at finite temperature, Quantum Sci. Technol. **9**, 015008 (2024).

[58] A. Bastianello, V. Alba, and J.-S. Caux, Generalized hydrodynamics with space-time inhomogeneous interactions, Phys. Rev. Lett. **123**, 130602 (2019).

[59] M. Collura, A. De Luca, P. Calabrese, and J. Dubail, Domain wall melting in the spin-$\frac{1}{2}$ xxz spin chain: Emergent luttinger liquid with a fractal quasiparticle charge, Phys. Rev. B **102**, 180409(R) (2020).

[60] R. Koch, A. Bastianello, and J.-S. Caux, Adiabatic formation of bound states in the one-dimensional bose gas, Phys. Rev. B **103**, 165121 (2021).

[61] J. Durnin, A. De Luca, J. De Nardis, and B. Doyon, Diffusive hydrodynamics of inhomogenous Hamiltonians, J. Phys. A: Math. Theor. **54**, 494001 (2021).

[62] V. Alba, B. Bertini, M. Fagotti, L. Piroli, and P. Ruggiero, Generalized-hydrodynamic approach to inhomogeneous quenches: correlations, entanglement and quantum effects, J. Stat. Mech.: Theory Exp. (2021) 114004.

[63] A. Bastianello, A. De Luca, and R. Vasseur, Hydrodynamics of weak integrability breaking, J. Stat. Mech.: Theory Exp. (2021) 114003.

[64] B. S. Shastry and B. Sutherland, Twisted boundary conditions and effective mass in heisenberg-ising and hubbard rings, Phys. Rev. Lett. **65**, 243 (1990).

[65] M. A. Cazalilla, R. Citro, T. Giamarchi, E. Orignac, and M. Rigol, One dimensional bosons: From condensed matter systems to ultracold gases, Rev. Mod. Phys. **83**, 1405 (2011).

[66] T. A. Brody, J. Flores, J. B. French, P. A. Mello, A. Pandey, and S. S. M. Wong, Random-matrix physics: spectrum and strength fluctuations, Rev. Mod. Phys. **53**, 385 (1981).

[67] L. F. Santos and M. Rigol, Onset of quantum chaos in one-dimensional bosonic and fermionic systems and its relation to thermalization, Phys. Rev. E **81**, 036206 (2010).

[68] P. Sierant and J. Zakrzewski, Level statistics across the many-body localization transition, Phys. Rev. B **99**, 104205 (2019).

[69] A. Pandey and R. Ramaswamy, Level spacings for harmonic-oscillator systems, Phys. Rev. A **43**, 4237 (1991).

[70] P. R. Zangara, A. D. Dente, E. J. Torres-Herrera, H. M. Pastawski, A. Iucci, and L. F. Santos, Time fluctuations in isolated quantum systems of interacting particles, Phys. Rev. E **88**, 032913 (2013).

[71] M. A. Garcia-March, S. van Frank, M. Bonneau, J. Schmiedmayer, M. Lewenstein, and L. F. Santos, Relaxation, chaos, and thermalization in a three-mode model of a Bose-Einstein condensate, New J. Phys. **20**, 113039 (2018).

[72] T. Guhr, A. Müller-Groeling, and H. A. Weidenmüller, Random-matrix theories in quantum physics: common concepts, Phys. Rep. **299**, 189 (1998).

[73] V. Oganesyan and D. A. Huse, Localization of interacting fermions at high temperature, Phys. Rev. B **75**, 155111 (2007).

[74] Y. Y. Atas, E. Bogomolny, O. Giraud, and G. Roux, Distribution of the ratio of consecutive level spacings in random matrix ensembles, Phys. Rev. Lett. **110**, 084101 (2013).

[75] D. J. Luitz, N. Laflorencie, and F. Alet, Many-body localization edge in the random-field heisenberg chain, Phys. Rev. B **91**, 081103(R) (2015).

[76] P. Sierant, M. Lewenstein, and J. Zakrzewski, Polynomially filtered exact diagonalization approach to many-body localization, Phys. Rev. Lett. **125**, 156601 (2020).

[77] J. Šuntajs, J. Bonča, T. Prosen, and L. Vidmar, Quantum chaos challenges many-body localization, Phys. Rev. E **102**, 062144 (2020).

[78] P. Sierant, D. Delande, and J. Zakrzewski, Thouless time analysis of anderson and many-body localization transitions, Phys. Rev. Lett. **124**, 186601 (2020).

[79] D. A. Abanin, J. H. Bardarson, G. De Tomasi, S. Gopalakrishnan, V. Khemani, S. A. Parameswaran, F. Pollmann, A. C. Potter, M. Serbyn, and R. Vasseur, Distinguishing localization from chaos: Challenges in finite-size systems, Ann. Phys. (NY) **427**, 168415 (2021).

[80] M. Kiefer-Emmanouilidis, R. Unanyan, M. Fleischhauer, and J. Sirker, Evidence for unbounded growth of the number entropy in many-body localized phases, Phys. Rev. Lett. **124**, 243601 (2020).

[81] R. K. Panda, A. Scardicchio, M. Schulz, S. R. Taylor, and M. Žnidarič, Can we study the many-body localisation transition?, Europhys. Lett. **128**, 67003 (2020).

[82] P. Sierant, E. G. Lazo, M. Dalmonte, A. Scardicchio, and J. Zakrzewski, Constraint-induced delocalization, Phys. Rev. Lett. **127**, 126603 (2021).

[83] E. van Nieuwenburg, Y. Baum, and G. Refael, From Bloch oscillations to many-body localization in clean interacting systems, Proc. Natl. Acad. Sci. USA **116**, 9269 (2019).

[84] M. Schulz, C. A. Hooley, R. Moessner, and F. Pollmann, Stark many-body localization, Phys. Rev. Lett. **122**, 040606 (2019).

[85] T. Chanda, R. Yao, and J. Zakrzewski, Coexistence of localized and extended phases: Many-body localization in a harmonic trap, Phys. Rev. Res. **2**, 032039(R) (2020).

[86] R. Yao, T. Chanda, and J. Zakrzewski, Many-body localization in tilted and harmonic potentials, Phys. Rev. B **104**, 014201 (2021).

[87] M. S. Bahovadinov, D. V. Kurlov, S. I. Matveenko, B. L. Altshuler, and G. V. Shlyapnikov, Many-body localization

transition in a frustrated xy chain, Phys. Rev. B **106**, 075107 (2022).

[88] V. Khemani, M. Hermele, and R. Nandkishore, Localization from hilbert space shattering: From theory to physical realizations, Phys. Rev. B **101**, 174204 (2020).

[89] P. Sala, T. Rakovszky, R. Verresen, M. Knap, and F. Pollmann, Ergodicity breaking arising from hilbert space fragmentation in dipole-conserving hamiltonians, Phys. Rev. X **10**, 011047 (2020).

[90] Z. Lan, M. van Horssen, S. Powell, and J. P. Garrahan, Quantum slow relaxation and metastability due to dynamical constraints, Phys. Rev. Lett. **121**, 040603 (2018).

[91] W.-H. Li, X. Deng, and L. Santos, Hilbert space shattering and disorder-free localization in polar lattice gases, Phys. Rev. Lett. **127**, 260601 (2021).

[92] H. Korbmacher, P. Sierant, W. Li, X. Deng, J. Zakrzewski, and L. Santos, Lattice control of nonergodicity in a polar lattice gas, Phys. Rev. A **107**, 013301 (2023).

[93] S. Scherg, T. Kohlert, P. Sala, F. Pollmann, B. Hebbe Madhusudhana, I. Bloch, and M. Aidelsburger, Observing non-ergodicity due to kinetic constraints in tilted fermi-hubbard chains, Nat. Commun. **12**, 4490 (2021).

[94] T. Kohlert, S. Scherg, P. Sala, F. Pollmann, B. Hebbe Madhusudhana, I. Bloch, and M. Aidelsburger, Exploring the regime of fragmentation in strongly tilted fermi-hubbard chains, Phys. Rev. Lett. **130**, 010201 (2023).

[95] K. Mallayya and M. Rigol, Heating rates in periodically driven strongly interacting quantum many-body systems, Phys. Rev. Lett. **123**, 240603 (2019).

[96] P. C. Burke and M. Haque, Entropy and temperature in finite isolated quantum systems, Phys. Rev. E **107**, 034125 (2023).

[97] R. Mondaini and M. Rigol, Eigenstate thermalization in the two-dimensional transverse field Ising model. II. Off-diagonal matrix elements of observables, Phys. Rev. E **96**, 012157 (2017).

[98] F. H. L. Essler, S. Evangelisti, and M. Fagotti, Dynamical correlations after a quantum quench, Phys. Rev. Lett. **109**, 247206 (2012).

[99] M. Srednicki, The approach to thermal equilibrium in quantized chaotic systems, J. Phys. A: Math. Gen. **32**, 1163 (1999).

[100] C. Nation and D. Porras, Quantum chaotic fluctuation-dissipation theorem: Effective brownian motion in closed quantum systems, Phys. Rev. E **99**, 052139 (2019).

[101] J. D. Noh, T. Sagawa, and J. Yeo, Numerical verification of the fluctuation-dissipation theorem for isolated quantum systems, Phys. Rev. Lett. **125**, 050603 (2020).

[102] M. Serbyn, Z. Papić, and D. A. Abanin, Thouless energy and multifractality across the many-body localization transition, Phys. Rev. B **96**, 104201 (2017).

[103] L. Foini and J. Kurchan, Eigenstate thermalization hypothesis and out of time order correlators, Phys. Rev. E **99**, 042139 (2019).

[104] A. Chan, A. De Luca, and J. T. Chalker, Eigenstate correlations, thermalization, and the butterfly effect, Phys. Rev. Lett. **122**, 220601 (2019).

[105] M. Brenes, S. Pappalardi, M. T. Mitchison, J. Goold, and A. Silva, Out-of-time-order correlations and the fine structure of eigenstate thermalization, Phys. Rev. E **104**, 034120 (2021).

[106] J. Wang, M. H. Lamann, J. Richter, R. Steinigeweg, A. Dymarsky, and J. Gemmer, Eigenstate thermalization hypothesis and its deviations from random-matrix theory beyond the thermalization time, Phys. Rev. Lett. **128**, 180601 (2022).

[107] H. Kim, T. N. Ikeda, and D. A. Huse, Testing whether all eigenstates obey the eigenstate thermalization hypothesis, Phys. Rev. E **90**, 052105 (2014).

[108] D. J. Luitz, Long tail distributions near the many-body localization transition, Phys. Rev. B **93**, 134201 (2016).

[109] M. Mierzejewski and L. Vidmar, Quantitative impact of integrals of motion on the eigenstate thermalization hypothesis, Phys. Rev. Lett. **124**, 040603 (2020).

[110] The additional scale factor rises from the averaging of local operators and affects the operator norm $\|O\| = \sqrt{\mathrm{tr}\, O^\dagger O}/D$. For a local operator like $\sigma_i^x \sigma_{i+2}^x$, the norm scales as $D^{-1/2}$, whereas for averaged operators like $\hat{T}$ and $\hat{Z}$, it scales as $(ND)^{-1/2}$. This extra factor $N^{-1/2}$ should be reflected in the adjusted ETH ansatz.

[111] H. Kim and D. A. Huse, Ballistic spreading of entanglement in a diffusive nonintegrable system, Phys. Rev. Lett. **111**, 127205 (2013).

[112] D. N. Page, Average entropy of a subsystem, Phys. Rev. Lett. **71**, 1291 (1993).

[113] L. Vidmar and M. Rigol, Entanglement entropy of eigenstates of quantum chaotic hamiltonians, Phys. Rev. Lett. **119**, 220603 (2017).

[114] Y. Huang, Universal eigenstate entanglement of chaotic local Hamiltonians, Nucl. Phys. B **938**, 594 (2019).

[115] G. De Chiara, S. Montangero, P. Calabrese, and R. Fazio, Entanglement entropy dynamics of heisenberg chains, J. Stat. Mech.: Theory Exp. (2006) P03001.

[116] M. Žnidarič, T. Prosen, and P. Prelovšek, Many-body localization in the Heisenberg XXZ magnet in a random field, Phys. Rev. B **77**, 064426 (2008).

[117] J. H. Bardarson, F. Pollmann, and J. E. Moore, Unbounded growth of entanglement in models of many-body localization, Phys. Rev. Lett. **109**, 017202 (2012).

[118] M. Serbyn, Z. Papić, and D. A. Abanin, Universal slow growth of entanglement in interacting strongly disordered systems, Phys. Rev. Lett. **110**, 260601 (2013).

[119] F. Iemini, A. Russomanno, D. Rossini, A. Scardicchio, and R. Fazio, Signatures of many-body localization in the dynamics of two-site entanglement, Phys. Rev. B **94**, 214206 (2016).

[120] M. Serbyn, Z. Papić, and D. A. Abanin, Local conservation laws and the structure of the many-body localized states, Phys. Rev. Lett. **111**, 127201 (2013).

[121] D. A. Huse, R. Nandkishore, and V. Oganesyan, Phenomenology of fully many-body-localized systems, Phys. Rev. B **90**, 174202 (2014).

[122] V. Ros, M. Mueller, and A. Scardicchio, Integrals of motion in the many-body localized phase, Nucl. Phys. B **891**, 420 (2015).

[123] M. Mierzejewski, M. Kozarzewski, and P. Prelovšek, Counting local integrals of motion in disordered spinless-fermion and Hubbard chains, Phys. Rev. B **97**, 064204 (2018).

[124] V. V. Flambaum and F. M. Izrailev, Unconventional decay law for excited states in closed many-body systems, Phys. Rev. E **64**, 026124 (2001).

[125] F. M. Izrailev and A. Castañeda-Mendoza, Return probability: Exponential versus Gaussian decay, Phys. Lett. A **350**, 355 (2006).

[126] E. J. Torres-Herrera and L. F. Santos, Quench dynamics of isolated many-body quantum systems, Phys. Rev. A **89**, 043620 (2014).

[127] M. Távora, E. J. Torres-Herrera, and L. F. Santos, Inevitable power-law behavior of isolated many-body quantum systems and how it anticipates thermalization, Phys. Rev. A **94**, 041603(R) (2016).

[128] M. Schiulaz, E. J. Torres-Herrera, and L. F. Santos, Thouless and relaxation time scales in many-body quantum systems, Phys. Rev. B **99**, 174313 (2019).

[129] T. L. M. Lezama, E. J. Torres-Herrera, F. Perez-Bernal, Y. Bar Lev, and L. F. Santos, Equilibration time in many-body quantum systems, Phys. Rev. B **104**, 085117 (2021).

[130] D. J. Luitz, N. Laflorencie, and F. Alet, Extended slow dynamical regime close to the many-body localization transition, Phys. Rev. B **93**, 060201(R) (2016).

[131] S. Bera, G. De Tomasi, F. Weiner, and F. Evers, Density propagator for many-body localization: Finite-size effects, transient subdiffusion, and exponential decay, Phys. Rev. Lett. **118**, 196801 (2017).

[132] P. Sierant and J. Zakrzewski, Challenges to observation of many-body localization, Phys. Rev. B **105**, 224203 (2022).

[133] P. Scholl, H. J. Williams, G. Bornet, F. Wallner, D. Barredo, L. Henriet, A. Signoles, C. Hainaut, T. Franz, S. Geier, A. Tebben, A. Salzinger, G. Zürn, T. Lahaye, M. Weidemüller, and A. Browaeys, Microwave engineering of programmable xxz hamiltonians in arrays of rydberg atoms, PRX Quantum **3**, 020303 (2022).

[134] C.-L. Hung, A. González-Tudela, J. I. Cirac, and H. J. Kimble, Quantum spin dynamics with pairwise-tunable, long-range interactions, Proc. Natl. Acad. Sci. USA **113**, E4946 (2016).

[135] C. Tabares, A. Muñoz de las Heras, L. Tagliacozzo, D. Porras, and A. González-Tudela, Variational quantum simulators based on Waveguide QED, Phys. Rev. Lett. **131**, 073602 (2023).

[136] S. Notarnicola, A. Elben, T. Lahaye, A. Browaeys, S. Montangero, and B. Vermersch, A randomized measurement toolbox for an interacting Rydberg-atom quantum simulator, New J. Phys. **25**, 103006 (2023).

[137] D. Bluvstein, H. Levine, G. Semeghini, T. T. Wang, S. Ebadi, M. Kalinowski, A. Keesling, N. Maskara, H. Pichler, M. Greiner, V. Vuletić, and M. D. Lukin, A quantum processor based on coherent transport of entangled atom arrays, Nature (London) **604**, 451 (2022).

[138] P. Sierant, D. Delande, and J. Zakrzewski, Many-body localization due to random interactions, Phys. Rev. A **95**, 021601(R) (2017).

[139] Y. Bar Lev, D. R. Reichman, and Y. Sagi, Many-body localization in system with a completely delocalized single-particle spectrum, Phys. Rev. B **94**, 201116(R) (2016).

[140] X. Li, D.-L. Deng, Y.-L. Wu, and S. Das Sarma, Statistical bubble localization with random interactions, Phys. Rev. B **95**, 020201(R) (2017).

[141] P. Sierant and J. Zakrzewski, Many-body localization of bosons in optical lattices, New J. Phys. **20**, 043032 (2018).